Breast Cancer Treatment Using Automated Robot Support Technology For Mri Breast Biopsy

[1]G S Pradeep Ghantasala, [2]Nalli Vinaya Kumari
[1]Chitkara University Institute of Engineering and Technology,
Chitkara University, Punjab, India
[2]Malla Reddy Institute of Technology and Science, Hyderabad, Telangana, India
[1]ggspradeep@gmail.com, [2]v.vinayakumari@gmail.com

Corresponding Author : ggspradeep@gmail.com

Doi :

Keywords :

Robotic-Assisted Surgery, MRI, lesion, needle insertion, Tissue repair and reconstruction.

Abstract

The robot is intrinsically safe for MR except for the off-shelf needle. Under MRI direction, the robot can accurately locate lesions, raising tissue injury and the risk of false negatives. These results are positive for clinical research, enhancing the quality of healthcare on MRI-guided breast biopsies. The new robotic surgery studies in tissue repair and regeneration have been systematically reviewed and analyzed. Surgical robots may increase the accuracy of skin flaps and shorten the harvest time. Moreover, robotic surgery benefits from minimal trauma in the tissue and therefore forms a minimum scar. The IGAR (Automated Robot Picture Guided) is a robot platform Form able to perform clinical interventions under the image with high precision Leadership. IGAR is unique because it is compliant with MRI and Maintains safe operation, proper protection, high image quality and accuracy. Even in an imaging environment, robotic control.

One of the most commonly diagnosed forms of cancer in women is breast cancer with a reported 1,67 million new cases in 2012. Early cancer for optimizing the results of the patient. In screening programs, mammography is the main form of imaging followed by ultrasound. In people with an elevated risk of breast cancer, magnet resonance imaging (MRI) is also used (Gulotta G et al, 2018, Ghantasala, G. P., & Kumari, N. V,2021). Injuries not seen on mammograms or ultrasound can be observed on MRI with greater sensitivity than the two other imaging modalities. The additional radiation dose and the computed tomography are not regularly used for the screening of breast cancer, (G S Pradeep Ghantasala, D. Nageswara Rao, Mandal K , 2021).

But for mammography, a minimal added benefit. If a suspected lesion is found, the radiologist can opt for a tissue sample utilizing a biopsy and the diagnosis must be confirmed (G. S. Pradeep Ghantasala, Nalli Vinaya Kumari, 2020). The next step in the MRI assessment has been identified Suspicious injuries are ultrasound and ultrasound-guided biopsy targeted, if positive (P, Fichtinger G, Peters TM, et al, 2013). However, during ultrasound scanning, the radiologists are often unable to find the lesions detected at MRI. This requires an MRI-led biopsy. Due to the boring accessibility restrictions which require the patient to move inside and outside the scanner multiples, it is difficult to target the lesion precisely during this process. Discretion errors of up to 4 mm are also introduced when a positioning grid is used. In addition, suction

Figure 1: Pneumatic state-of-the-art pneumatic robots
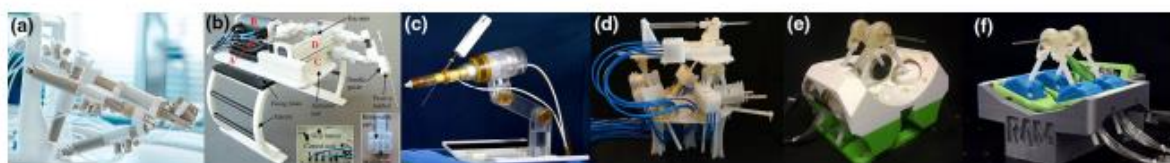
Other unintentional motions of the body can cause the displacement of the breast tissue. These factors may produce false-negative results or an ongoing procedure due to needle repositioning.

Figure 2: Stormram 4, with labelled parts and joints
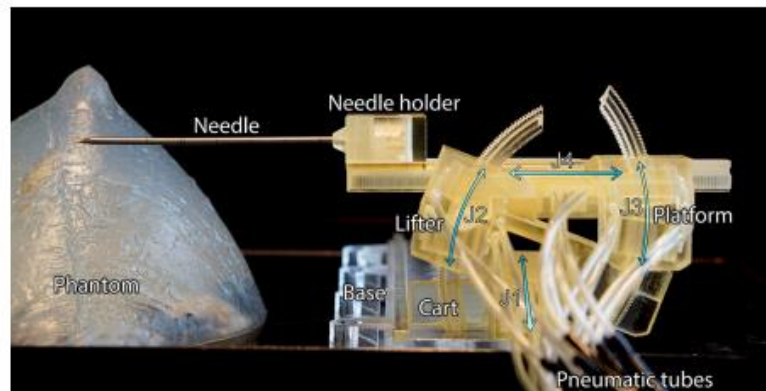
A safe MR robotics system can resolve the lack of an existing manual MRI-guided biopsy procedure. This system allows fast MRI feedback on biopsies in the boron of the scanner. Owing to improved accuracy, we predict that fewer samples are needed to minimize tissue damage and to shorten operating times. Given the changes that have been made in the past, the aim of Stormram 4 is to design and characterize a new MR-safe robotic system for breast biopsy, which increases its precision and workspace significantly over previous designs.

MR Classification

Three possible alternatives are defined by the ASTM F 2503 standard. Classification of RMDs: safe, conditional and dangerous RM. The secure MR classification based on scientific evidence (i.e. content composition) is based instead of the research results. This group consists primarily of non-metallic and non-magnetic compounds (Oleynikov D, Tsuda S, Gould J, et al, 2015). The MR designation, however, suggests that the system is stable only when it runs under these controlled conditions. Finally, the unclear MR classification indicates that in all the MRI environments the device is considered to pose a danger(Ghantasala, G. P., Kallam, S., Kumari, N. V., & Patan, R, 2020). This new standard tries to eliminate misunderstandings and mistakes resulting from outdated jargon that modern studies have to prevent. This new norm aims to reduce confusion and errors.

The State of the Art

A few MRI robots have been described in the literature. Due to interference in the magnetic field of the MRI scanner, the use of modern electromechanical motors is omitted. Different types of actuation have been explored: hydraulics, piezo motors, ultrasound generators, ferromagnetic induction models, fluidic mobile drives, air turbines, direct-acting pneumatic tubes, and pneumatically steps (Bhowmik, C., Ghantasala, G. P., & AnuRadha, R, 2021). The pneumatic stepper motor operation provides various advantages over other categories: inherent MR safety, small air leakage tolerant pneumatic motors can be controlled in medical applications through pneumatic multiples and feed-forward control methods are implemented (Lane T. A, 2018, Diana M, J, 2015). Figure 1a–1f shows six MRI pneumatic robots found in the literature. (a) the MR stable remote-controlled parallel guide handler2 built and tested by Bosboom et al. There are five stepper engines. Each engine has a rod in the helical hole, which alternates into a rod torque in four single-acting cylinders. The robot takes around six minutes to handle, which makes the push of the needle to the controlled location comparatively fast. Four direct pneumatic cylinders have been designed to control the piston precisely to linear, stepping veins aimed at destination venous motors control the relative size of the robot. Six are a Stewart frame and the seventh longitudinally position the screw. 5 The needle-led robot for laser removal of hepatic tumours has been designed. Figure 1(e), displays Stormram 2 that is powered by smaller, lighter stepper motors incorporated in the ball joints. Messages showed that lesions with a relatively low accuracy of 6.0 ± 2.0 mm, 1,7 mostly through joint clearance, can be treated in the womb. Figure1(f) shows that Stormram 3 is similar in scale and film style to its predecessor. While the exactness has improved to 2 mm and a stronger handle actuator that supplies up to 70 N of force8 has been mounted, the parallel film structure has provided a complex control system and an optimized working area.

Methods

It explains the architecture and assessment of Stormram 4, which is seen in the figure. 2. A serial film chain based on the combination of linear and pneumatic stepper motors is the solution. It is intended in particular to address scale, difficulty, preciseness and room to accommodate the shortcomings of state-of-the-art MRI robots. An enlarged workspace is created instead of using a parallel-serial film chain (Bhowmik, C., Ghantasala, G. P., & AnuRadha, R, 2021). High precision is achieved by combining linear step dimensions of 0, 25 mm and corner step sizes of 0, 25 rear-blast-free joints (i.e., 0,54 mm scroll in a radius of 100 mm). It provides good rigidity due to the compactness of the robot and the drive of revolutionary connections

within 50 mm of its axis. Lightweight (2 mm) pneumatic pipes allow unrestricted movement of various levels of freedom near the system. In addition to bench tests, detailed MRI tests are recorded. For autonomous operators, an automatic needle sensing algorithm was developed to reliably confirm the location of the needle(Yuan, Chow RC, Jackson RC, and al, 2018).

Kinematic Design

The film serial operator is Stormram 4. Every motor is powered by a four-degree pneumatic stepper motor. The robot measures 72 9 51 9 40 mm (not including needles and racks) at home. Identify the names of the various robot parts. 2. It consists of a linear board, on which the carriage can be pushed back and forth over a 160 mm span, with a linear phase motor. A revolving joint J2 driven by a motor with a curved stepper range of 47 is connected to the base and the lifter (Clemens MW, Kronowitz S, Selber JC, 2014). The lift and platform are connected by a new rotating J3, also powered by a curved step engine with a range of 38. When the two rotating joints are connected, the platform can be moved upwards and downwards (but not horizontally) (Self-JC, Baumann DP, Holsinger FC, 2012). Finally, a linear stepper motor is pushed to the frame and creates the J4 joint through a length of 80 mm.

Pneumatic stepper motors

Two stepper motors are available for the Stormram 4. The T-26 powers a prismatic joint, while the C-30 curved motor is designed to control a revolving joint. The main difference is that the radius of the rack curvature affects the geometries and pistons simultaneously. The two engines are equally designed and assembled (Chih-Sheng L, Knight D, et al, 2018). Displays internally the C-30 curved motor. Each (green) column operates with both columns. Pressurized air into either end of the cylinder, when the piston is pushed up and down. Silicone block seals on the air leak on the columns. There is a panel.

With two jaws (sets of teeth) inside, the rack is pushed onto the rack by a wedge mechanism and moves in small steps to the left or right. The curved rack has a width of 50 mm and can be supported by a harness joint with a well-defined rotary axis and significantly increase the   stability   of   the   mechanism.

Fabrication

The bulk of robotic parts are designed and assembled to the contents of FullCure720. Compared to silicone rubber with 0.5 mm the display was a laser. In the two hinge articulation areas between the cart, acrylic rods with a thickness of 3 mm and lifting components and platform components were used at points A and Fig. 4. These rods have been grafted with silicone to allow enough rotation. Small friction and no measurable game. The polyurethane tube provides air from the valve collector for the pressurizing device. A silicone grid for moving components is used as a lubricant. The MR of the robot, Conditional Bard 14 G 100 mm (Bard, Inc., Murray Hill, NJ, USA), was fitted in the study. The symmetrical tip and needle can bend due to their diamond shape so that the needle is taken straight through all experiments. The needle chosen is not an integral part of the robot, because the needle can be replaced by a needle, for example, to meet the conditions of a certain MRI scanner. The robot may be classified as a healthy MR depending on the entire composition of the material of the robot (except the needle). A laser-cut acrylic platform with a linear rail and trail guide is the basis of the robot (SH, S, JH, Kim and others, 2006). A polylactic acid table with 10 fish oil capsules, like fiduces, is added to the basis for identification and orientation. The process of cooling down was fantastically accompanied by 4-10 lesions (5-20 mm) each. The filling of a hot 3 D mold PVC-plastizer mix produced by mathematic description was used to create different fantasies. The ghost strengthens into an elastic mass with randomly spread lesions during this process. In certain sequences, the lesions contained either fish oil capsules or fragments of rigid PVC, which are relatively robust and MRI separated.

Conclusion

The average site processing time is estimated at 6:38 minutes, including robot operation and confirmatory monitoring. This corresponds to the total time of a 3D bSSFP scan with pre-scan image calibration and reconstruction. Faster scans with the same SNR and resolution reduce the runtime through a strong MRI (i.e. 3 T) magnetic field scanner. To push the needle from one target to another, the robot takes less than 1:30. This is mainly due to the insertion of the needle of 2 mm / s and the retraction up to 80 mm. It is very useful to have two phases motors combined with different phase sizes in a single linear connection, such that the same step frequent 8 Hz under load is generated at both large and small phases. Further developments are necessary before clinical trials. A built-in breast attachment system must be established for an RF breast belt. Stimulate the breast of a patient. A biopsy gun shall be installed on the robot to collect tissue samples. Structural rigidity must be improved. Keep high accuracy

constantly. For sterilization and possible failure of the system, safety mechanisms and procedures need to be developed. The robotic system has strong clinical potential in vivo when all these components are combined.

References

Gulotta G et al, 2018. Marino MV, Shabat G. From illusion to fact: a short history of robotic operation. Surg Innovation. Surg Innovation. 28:291e296. 2018. .org/10.1177/ 1553350618771417.

P, Fichtinger G, Peters TM, et al, 2013. Abolmaesumi. Introduction to the Surgical Robot Special Section. Engineering IEEE Trans Biomed. 2013;60:41122. https:/doi, organ/10/10-101-tbme.2013.23324.2.

Oleynikov D, Tsuda S, Gould J, et al. 2015. *The safety and efficacy analysis of SAGES TAVAC is*: da
Vinci ® Surgical System (Sunnyvale, CA). Endosc appear. 29:2873e2884. https:/doi.org/10.1007/s0022-224-y.

Lane T. A, 2018. short robotic operation history. *Ann R Coll Surg Engl*. English. 2018;100:34. 2018. https:/doi.org(10.1308).supp1.5. [3].

Diana M, J, 2015. Robotic operation. *Diana M. South of France*. 2015;102: e15. Hamstring.org/ 10.1002 / bjs.9711.

Yuan, Chow RC, Jackson RC, and al, 2018. Visual dynamic suture thread tracking in real-time. *IEEE Trans Sci Eng.* Trans Sci. 2018,1078 and 1090:15. TASE / MSFF. 2017.2726689. https:/ doi.org/10.1109.

Clemens MW, Kronowitz S, Selber JC, 2014. *Robotic aided latissimus dorsi harvest in delayed rapid repair of the breasts*.. 2014;20e25:28. Semin Plast Surg. Hammock.org/10.1055 / s-0034-1368163.

Self-JC, Baumann DP, Holsinger FC, 2012. Latissimus robotic latissimus dorsi: series of cases. 2012;129:1305e1312. Plast Reconstr Surg. https:/doi.org/10.11824ecc0b/SRS.0b0213e31823.

Chih-Sheng L, Knight D, et al. 2018. Louis V. A model of porcine for the collection of robotic rectal muscle exercise. Plast Esthet's Ann Chir. 2018;63: 113. The file is at the bottom. 2017.11.010 anplas.

SH, S, JH, Kim and others, 2006. Compared to traditional laparoscopic rectal cancer surgery, robotic: systemic review and meta-analysis. Treat Res Ann Surg. 2015;89:206. 2015. HTTPs:/doi.org/10.428/astr.2006-04-08-29.

G S Pradeep Ghantasala, D. Nageswara Rao, Mandal K (2021) MACHINE LEARNING ALGORITHMS BASED BREAST CANCER PREDICTION MODEL. *Journal of Cardiovascular Disease Research*, 12 (4), 50-56. doi:10.31838/jcdr.2021.12.04.04

Kishore, D. R., Syeda, N., Suneetha, D., Kumari, C. S., & Ghantasala, G. P. (2021). Multi Scale Image Fusion through Laplacian Pyramid and Deep Learning on Thermal Images. *Annals of the Romanian Society for Cell Biology*, 3728-3734.

Ghantasala, G. P., Kallam, S., Kumari, N. V., & Patan, R, 2020. Texture Recognition and Image Smoothing for Microcalcification and Mass Detection in Abnormal Region. In *2020 International Conference on Computer Science, Engineering and Applications (ICCSEA)* (pp. 1-6). IEEE. (Bhowmik, C., Ghantasala, G. P., & AnuRadha, R, 2021). A Comparison of Various Data Mining Algorithms to Distinguish Mammogram Calcification Using Computer-Aided Testing Tools. In *Proceedings of the Second International Conference on Information Management and Machine Intelligence* (pp. 537-546). Springer, Singapore.

Ghantasala, G. P., & Kumari, N. V. (2021). Identification of Normal and Abnormal Mammographic Images Using Deep Neural Network. *Asian Journal For Convergence In Technology (AJCT)*, *7*(1), 71-74.

G. S. Pradeep Ghantasala, Nalli Vinaya Kumari, 2020. Mammographic CADe and CADx for Identifying Microcalcification Using Support Vector Machine. *Journal of Communication Engineering & Systems*. 2020; 10(2): 9–16p.